INSTITUTE OF PHYSICS PUBLISHING JOURNAL OF PHYSICS B: ATOMIC, MOLECULAR AND OPTICAL PHYSICS

J. Phys. B: At. Mol. Opt. Phys. **36** (2003) 731–753 PII: S0953-4075(03)56799-2

Total electron scattering cross sections of He, Ne and Ar, in the energy range 4 eV–2 keV

W Y Baek and B Grosswendt

Physikalisch-Technische Bundesanstalt, Bundesallee 100, 38116 Braunschweig, Germany

E-mail: baek@ptb.de

Received 25 November 2002
Published 4 February 2003
Online at stacks.iop.org/JPhysB/36/731

Abstract

Total scattering cross sections of the rare gases He, Ne and Ar have been measured, for electrons in the energy range from 4 eV to 2 keV. The measurements were performed using a linear transmission device and an electron energy analyser, with an angular resolution better than 1.1×10^{-3} sr and with an energy resolution far below the first excitation threshold in the three atoms. The uncertainties of the experimental results are generally smaller than 3%. With a few exceptions, the present results are in good agreement with the data of other authors. Systematic deviations were found between the present results and the data available for the total scattering cross sections of He at high electron energies. The deviations increase with increasing energy and reach about 13% at 2 keV. It appears that different levels of the separation of forward-scattered electrons are responsible for these systematic deviations.

(Some figures in this article are in colour only in the electronic version)

1. Introduction

Scattering of electrons is one of the fundamental physical processes occurring either as a primary or as a secondary event whenever ionizing radiation interacts with matter. The knowledge of electron scattering cross sections is therefore indispensable for the quantitative analysis of radiation impact phenomena. Of practical importance in this context is the total electron scattering cross section, which is the sum of the integral cross sections of all types of interaction an electron may undergo in matter. It is, for instance, an essential input quantity for electron transport calculations by the Monte Carlo method, where it is used to determine the distance between subsequent interaction points and to compute the probabilities for specific interaction processes. It is also often applied in electron scattering experiments to convert relative cross sections into absolute values, profiting from the fact that it can be measured in absolute terms without any normalization procedure.

0953-4075/03/040731+23$30.00

Up to now, a great number of experiments (Trajmar and McConkey 1994, Zecca *et al* 1996) have been carried out to determine total electron scattering cross sections for a variety of atoms and molecules. A considerable number of these experiments focused on the measurement of total electron scattering cross sections of light noble-gas atoms. The interest in the light noble-gas atoms arose, on the one hand, because they were favoured as test systems for various theoretical models for electron–atom scattering. On the other hand, they are generally acknowledged to be one of the most accurately known cross sections, and therefore frequently serve as reference values for the determination of instrumental responses in electron scattering experiments.

Despite the particular interest, the actual data situation for the total electron scattering cross sections of light noble-gas atoms is not wholly satisfactory. The experimental data available still show rather large discrepancies. The results of different authors differ by up to about 20%, and differences in the order of 10%, which are significantly higher than the uncertainties claimed by the corresponding authors, are not rare, suggesting that the experimental data might be affected by unidentified systematic errors. Moreover, most authors measured the total electron scattering cross sections only for restricted energy ranges, so that the accuracy of the energy dependence obtained by combining the results of different authors may be limited by different potential systematic errors not properly taken into account. Finally, it is desirable to provide more data for electron energies above 1 keV, where only a few groups have measured the total electron scattering cross sections of light noble-gas atoms, differing by up to about 16% (Dalba *et al* 1979, 1981, Garcia *et al* 1986, Zecca *et al* 1987).

In view of these facts, total electron scattering cross sections of He, Ne and Ar were measured in the present work for electron energies from 4 eV to 2 keV, covering the major part of the energy range which is of interest both from the practical and theoretical points of view. The measurements were carried out by means of the linear transmission method. Particular attention was paid to the reduction of the experimental uncertainties, especially with respect to the separation of electrons scattered in the forward direction, which becomes increasingly important with rising electron energy.

2. Apparatus

A schematic diagram of the experimental set-up is depicted in figure 1. The apparatus consists of three main components: an electron gun, a scattering cell and an electron energy analyser, with a channel electron multiplier as detector. They were attached to a vacuum chamber. The electron gun delivered stable electron beams for energies between 20 eV and 5 keV, which were produced using a hairpin tungsten filament as cathode. The electrons emitted from the filament were accelerated to the adjusted end energy on their way to the anode and were then focused by an Einzel lens. Two pairs of deflection plates placed perpendicularly to each other at the end of the gun made it possible to change the beam direction. As described in more detail below, total scattering cross sections at energies smaller than 20 eV were measured by means of a 20 eV electron beam and by applying a negative voltage to the scattering cell.

The electron beam entered the scattering cell through an entrance aperture 0.5 mm in diameter, to undergo scattering processes with the atoms of interest. The scattering cell was of cylindrical form, and its symmetry axis was perpendicular to the beam direction. The electrons left the scattering cell through an exit aperture, also 0.5 mm in diameter. The distance between the midpoints of the entrance and exit apertures was 132 mm. The gas was fed into the scattering cell through a regulating valve, whose leak rate was adjustable between 10^{-9} and 600 mbar l s^{-1}. The gas streaming out through the apertures was removed by a turbomolecular pump, with a pumping speed of 2200 l s^{-1}, mounted on the vacuum chamber. The gas pressure

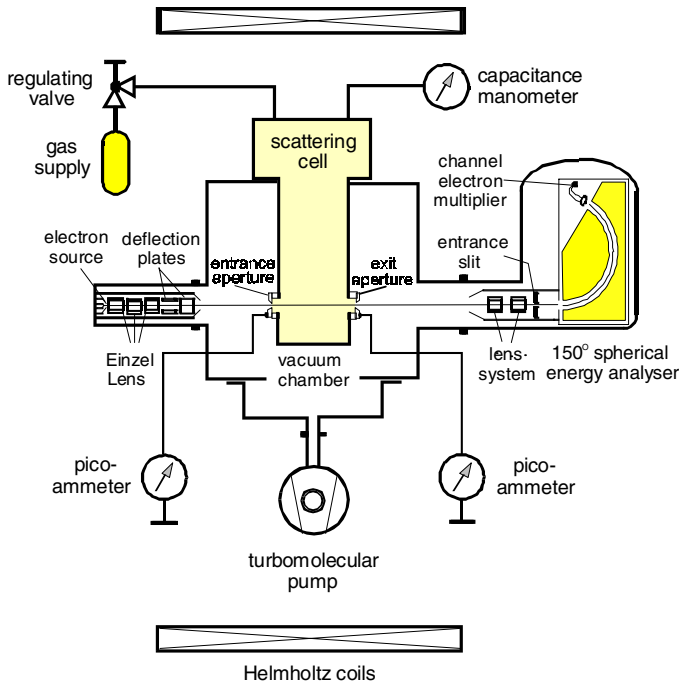

Figure 1. Schematic view of the experimental arrangement. The μ-metal cylinders used to shield the electron beam path against electromagnetic spikes are not plotted. The drawing is not to scale.

in the scattering cell was measured with a differential capacitance manometer, whose reading is almost independent of the gas type. The reference side of the manometer was connected to the high-vacuum region in the vacuum chamber, where the pressure was lower than 10^{-6} mbar throughout the measurement.

The reading of a capacitance manometer can deviate from the true value due to the so-called thermal transpiration effect (Edmonds and Hobson 1965), which ensues when the temperature of the gas is different from that of the gauge head, as was the case in the present experiment. The deviation depends on the ratio of the gas temperature to the temperature of the gauge head, which was kept constant at 46 °C in the present experiment, on the geometrical characteristics of the vacuum lines connecting the scattering cell with the gauge head and possibly also on the gas type. To determine the change of the pressure reading by the thermal transpiration effect, our pressure measuring system, i.e. the capacitance manometer with the vacuum lines, was calibrated for several gases using the absolute pressure standards provided by the vacuum metrology section of Physikalisch-Technische Bundesanstalt in Berlin, Germany. Figure 2 shows the correction factors, χ_B, i.e. the ratios of our manometer readings to the pressure standards for He and Ar, as a function of gas pressure. It can be seen from figure 2 that the correction factors for He are about 0.5% lower than those for Ar in the pressure range of interest to us, i.e., below 10^{-2} mbar. For Ne, we used the correction factors for He, assuming that the error arising from this is not greater than 0.5%, which was taken into account in the analysis of the uncertainties.

The electrons leaving the scattering cell were analysed with respect to their energy in the electron energy analyser, which consists of a 150° spherical condenser with a mean radius of 100 mm. It is provided with an entrance and an exit slit, 4 mm in width and 18 mm in

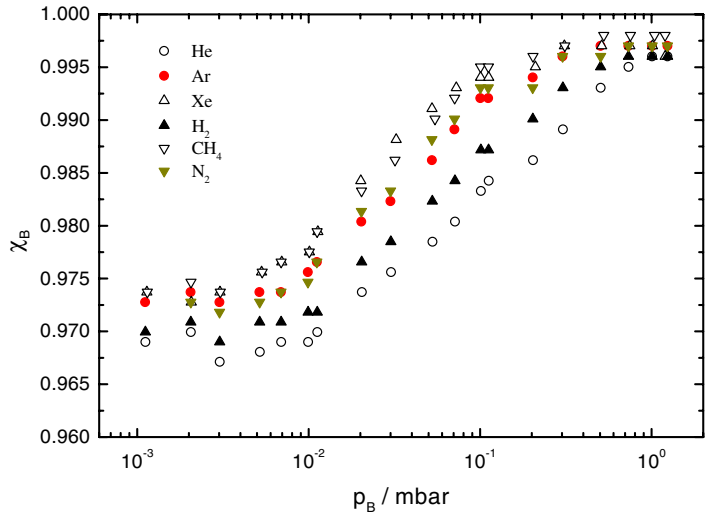

Figure 2. Correction factors, χ_B, for the pressure reading of the capacitance manometer used in the present experiment. The correction factors were determined by comparing the reading values, p_B, of the capacitance manometer used in this work with the pressure standards, p_N, provided by the vacuum metrology section of Physikalisch-Technische Bundesanstalt in Berlin, Germany. Plotted are the ratios, $\chi_B = p_N/p_B$, for several gases at different pressures. The uncertainties of the correction factors amount to 0.6% at $p_B \approx 1.0 \times 10^{-3}$ mbar and to about 0.4% at pressures $p_B \geqslant 2.0 \times 10^{-3}$ mbar.

height. The electrons with energies equal to the adjustable pass energy of the analyser move close to the centre orbit and leave the condenser through the exit slit, to be detected by the channel electron multiplier. In the present experiment, the focusing lens of the energy analyser was switched off in order to prevent a deterioration of the angular resolution due to electron focusing. The distance between the exit aperture of the scattering cell and the entrance slit of the analyser amounted to 318 mm, giving a geometrical value of 7.1×10^{-4} sr for the solid angle subtended by the entrance slit. Applying a retardation voltage to the entrance slit of the analyser, the energy resolution full width at half maximum (FWHM) was adjusted to less than 1 eV, which is much smaller than the lowest excitation energy in the three noble-gas atoms. This means that all electrons scattered inelastically can be completely separated from the non-scattered ones if the pass energy of the analyser is set equal to the primary electron energy. It is worthwhile mentioning that the application of a retardation voltage also leads to an improvement of the angular resolution.

The whole experimental area was surrounded by three orthogonal pairs of Helmholtz coils to compensate the Earth's magnetic field. Additionally, μ-metal cylinders 1 mm in thickness were used to shield the electron beam path against electromagnetic spikes. The residual field inside the μ-metal cylinders was smaller than 1 μT.

3. Experimental procedure

The determination of the total electron scattering cross section, σ, was based on Beer's attenuation law:

$$c = c_0 \exp(-\sigma n L), \tag{1}$$

where c and c_0 are the count rates of electrons detected after having traversed the scattering cell at the number density n and zero, respectively. The thickness of the gas layer, L, is equal to the length of the scattering cell in the beam direction, which is 132 mm as described above. The number density, n, was calculated from the gas pressure, p, in the scattering cell using the ideal gas law $n = p/(k_B\Theta)$, where k_B is the Boltzmann constant and Θ the absolute gas temperature. Due to the gas streaming out through the apertures, the number density near the apertures deviates from n. The inaccuracy arising from this inhomogeneous number density distribution is discussed below. In the following, it is assumed that the temperature of the gas is equal to that of the environment. The maximal pressure in the scattering cell during the measurement was between 10^{-3} and 10^{-2} mbar, depending on the gas type. It was chosen such that the beam attenuation did not exceed 60%, to keep multiple-scattering effects as small as possible.

The application of equation (1) presupposes that the primary electron beam current remains constant during the measurement of the beam attenuation as a function of the gas pressure in the scattering cell. To avoid errors due to a temporal fluctuation of the primary electron beam current, the current of the outer part of the beam striking the entrance aperture was measured and then used to normalize the detector count rate as described below. The beam current was adjusted such that on the one hand the gain of the channel electron multiplier, which begins to noticeably decrease with the increasing count rate above about 5×10^4 s^{-1}, did not much differ from the plateau where the gain is nearly independent of the count rate, and on the other hand it was at least two orders of magnitude higher than the leakage current, to keep the relative uncertainty of the current measurement below 1%. In most cases, this could be achieved with a beam current in the range of 1 pA.

The electron gun used in the present work is capable of delivering stable electron beams only for energies higher than 20 eV. In order to use the just stable 20 eV electron beam for the measurement of total electron scattering cross sections below 20 eV, the scattering cell was electrically isolated from the bulk and negatively biased, as shown in figure 3. When a negative voltage of U_{ch} is applied to the scattering cell, the electrons of the initial energy T_0 are slowed down en route to the entrance aperture of the scattering cell and undergo scattering processes at reduced energy, which in the first order is equal to T as defined by equation (2):

$$T = T_0 + eU_{ch}. \tag{2}$$

After leaving the scattering cell, the electrons are re-accelerated to the initial energy, T, on the way to the energy analyser. Therefore, keeping the initial electron and the pass energy of the analyser constant, the total electron scattering cross sections for different electron energies can be measured by varying the potential, U_{ch}, of the scattering cell.

The exact value of the electron energy in the scattering cell, especially in the area close to the apertures, is expected to be different from T, because of the penetration of the bulk potential into the scattering cell. Therefore, the accuracy of equation (2) was checked by measuring the energy dependence of the total electron scattering cross sections of N_2 in the energy range 1–4 eV, where several peaks occur due to the vibrational excitations of the negative-ion state $^2\prod_g$. Figure 4 shows the present results, after a horizontal shift by 0.25 eV to higher energies, in comparison with the data of Kennerly (1980), who measured the total electron scattering cross sections of N_2 using a time-of-flight spectrometer. The dashed curve was obtained by convolution of the data of Kennerly (1980) with a Gaussian curve with the FWHM of 0.15 eV, which corresponds to the energy width of the primary electron beam used in this work, and by a subsequent normalization of the convoluted data to the present results. It can be seen from figure 4 that the peak positions of the dashed curve agree reasonably well with those of the present results after the horizontal shift by 0.25 eV. Assuming that the energy distribution of the

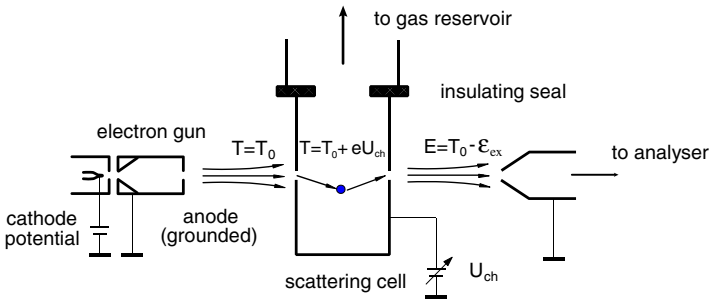

Figure 3. Electrical configuration used for the measurement of the total electron scattering cross sections below 20 eV. The scattering cell was electrically isolated from the bulk and negatively biased with respect to the grounded anode of the electron gun. An electron with the initial energy T_0 moves in the scattering cell at the reduced energy $T = T_0 + eU_{ch}$ and enters the electron energy analyser either at the initial energy, T_0, or at initial energy minus the excitation energy, $T_0 - \varepsilon_{ex}$, depending on the scattering history. The Einzel lens and deflection plates in the electron gun are not drawn but were used in the experiment.

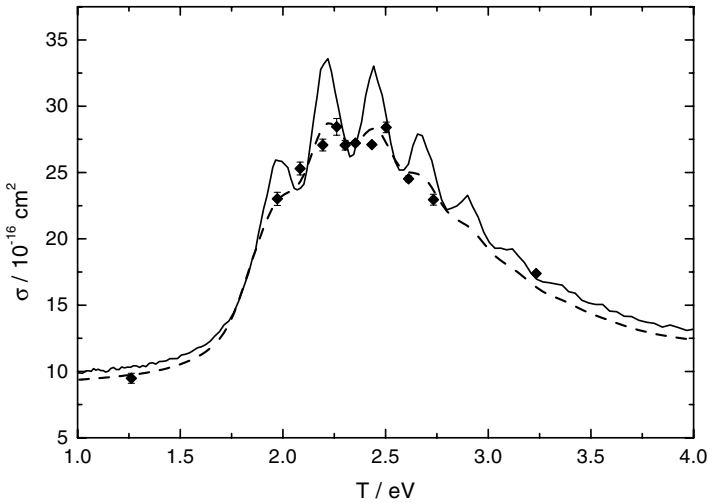

Figure 4. Peaks in the total electron scattering cross sections of N_2 in the energy region around 2 eV due to the vibrational excitations of the negative-ion state $^2\Pi_g$. The results of the present work obtained with the experimental arrangement shown in figure 3 and horizontally shifted by 0.25 eV are marked by the symbol –♦–. The unbroken curve represents the data of Kennerly (1980). The dashed curve depicts the convolution of the data of Kennerly (1980) by a Gaussian curve with the FWHM of 0.15 eV. For a better optical comparison, the maximum of this curve is adjusted to that of the present results by dividing the convoluted data of Kennerly (1980) by a factor of 1.06.

data of Kennerly (1980) is correct, the energy determination by equation (2) is in the following considered to be accurate within the uncertainty of 0.25 eV. It is worthwhile mentioning that the primary energies above 20 eV were determined by applying the retarding field method (Fox *et al* 1951), with a relative uncertainty smaller than 0.3%.

Due to the negative biasing of the scattering cell, the electrons moving in the direction to the grounded energy analyser are focused, which may result in a poorer angular resolution and, consequently, in the reduction of the measured total scattering cross section. The numerical simulation of the electron paths in the region between the scattering cell and the

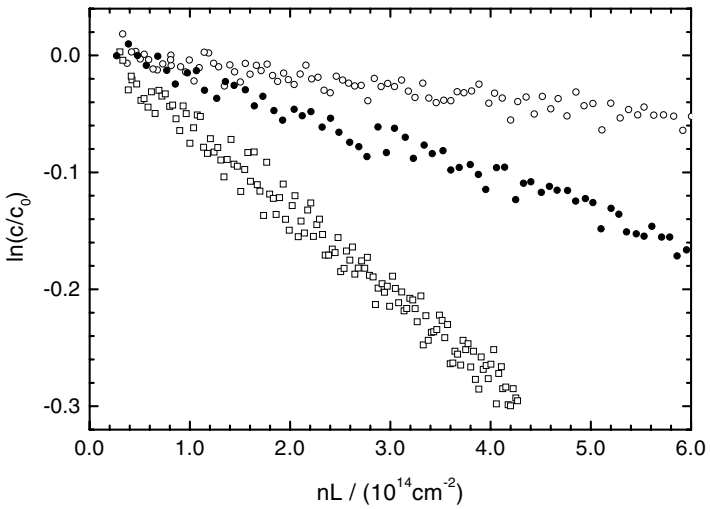

Figure 5. Attenuation of a 100 eV electron beam in He (○), Ne (●) and Ar (□) as a function of the number of atoms per area in the scattering cell. The letters c_0 and c denote the detector count rate of electrons after passage through the scattering cell at the number density zero and n, respectively.

energy analyser revealed that the angular resolution of the energy analyser deteriorates from the above-mentioned value of 7.1×10^{-4} to 1.1×10^{-3} sr in the worst case, occurring at $T = 4$ eV. The relative reduction of the total scattering cross section by this angular resolution, which was estimated using the differential elastic scattering cross sections of Fon *et al* (1981) for He, of Saha (1989) for Ne and of Fon *et al* (1983) for Ar, is in the order of 0.1% and negligible in comparison with other uncertainties specified below. It should be mentioned that the deterioration of the angular resolution does not raise the detection of electrons scattered inelastically, because of the energy selection by the analyser.

For each energy and gas, the measurement was usually repeated ten times to obtain enough samples for a statistical analysis. An example of the measurement is shown in figure 5, where the attenuations of a 100 eV electron beam in the three gases, He, Ne and Ar, are plotted versus the number of atoms per area, nL. Figure 5 clearly demonstrates that, in a logarithmic scale, the electron beam current decreases linearly with the increasing number density in the scattering cell. The different rates of decline indicate different total scattering cross sections of the three gases.

4. Data evaluation and uncertainty analysis

Applying equation (1) to determine total scattering cross sections requires that the electron count rate, c, change only with the number density, n, of the gas atoms in the scattering cell. In practice, however, this requirement can scarcely be met, because a number of different experimental effects influence the electron count rate. For instance, it can be changed by a temporal fluctuation of the primary electron beam current. Furthermore, the scattering of electrons by the gas atoms effusing through the apertures of the scattering cell may lead to an additional decrease in the count rate. For a precise determination of total electron scattering cross sections, it is necessary for these experimental effects to be included in the data evaluation. For this purpose, an evaluation model was derived, which comprises additional

terms representing the experimental effects:

$$\sigma(T) = k_1 k_2 k_3 m(T) \tag{3}$$

with

$$k_1 = 1 + \frac{n}{m(T)} \int_0^L \mathrm{d}z \int_{\Delta\Omega(z)} \mathrm{d}\Omega \, \frac{\mathrm{d}\sigma_{el}}{\mathrm{d}\Omega}, \tag{4}$$

$$k_2 = 1 - \frac{\sigma_R}{\sigma} \frac{p_R}{p}. \tag{5}$$

The factor k_1 corrects for the increase in the detector count rate by electrons scattered elastically in the forward direction and counted because of the finite solid angle of the detector. This increase in the detector count rate is connected with a lowering of the uncorrected total scattering cross section $m(T)$ in comparison with the true value. The value of the factor k_1 was estimated by means of the optical theorem (Bransden and Joachain 1983) for elastic scattering of electrons. The estimate for the present experimental arrangement revealed that k_1 deviates from unity by less than 0.001 in most cases. The factor k_2 was inserted to take into account the additional attenuation of the electron beam by residual gas in the scattering cell. The partial pressure of the residual gas was measured using a quadrupole mass analyser. The value of k_2 lies between 0.99 and 1.0 for He and is almost 1 for the other two gases.

The gas atoms streaming out through the entrance aperture of the scattering cell into the electron gun caused a widening and displacement of the electron beam, which both increased with increasing gas pressure in the cell. This led to an additional reduction of the detector count rate at a given gas pressure in the scattering cell and, consequently, to a counterfeit increase in the total electron scattering cross section, which was corrected by the insertion of the factor k_3. The factor k_3 was determined by re-adjusting the focusing and deflection voltage in the electron gun and then comparing the detector count rate with that before the re-adjustment. The value of k_3 lies between 0.99 and 1.0.

Unfortunately, the values of the three correction factors are not exactly known for all measurements, with the consequence that the amount of the corrections, i.e. the correction factors minus one, is comparable to their uncertainties. Therefore, we set the values of the correction factors to 1 and considered them in the analysis of the uncertainty, where the uncertainties $u(k_i)$ of the correction factors were set to the maximal differences of their values from 1: $u(k_1) = 10^{-3}$, $u(k_2) = 10^{-2}$ for He and $u(k_2) = 0$ for the other two gases and $u(k_3) = 10^{-2}$. The uncertainty of k_1 is of type B whereas those of k_2 and k_3 are of type A (*Guide to the Expression of Uncertainty in Measurement* 1993).

As mentioned above, the measurement of total electron scattering cross sections was repeated ten times for every electron energy and gas type. Each of the ten measurement cycles usually consists of more than 100 data vectors whose components are the electron count rate, the gas pressure in the scattering cell, the primary electron beam current at the entrance aperture etc. The uncorrected total electron scattering cross section, $m(T)$, was determined from the results of the ten measurement cycles, using the weighted average,

$$m(T) = \frac{\sum_i m_i / u^2(m_i)}{\sum_i 1/u^2(m_i)}. \tag{6}$$

The result m_i of the measurement cycle i was determined using a linear regression analysis on the basis of equation (1):

$$Y_i = a_i - m_i X_i, \tag{7}$$

where the experimental values of X_i and Y_i at the jth data point are given by

$$x_{ij} = (n_e L)_{ij} \qquad \text{and} \qquad y_{ij} = \ln(q/q_0)_{ij}, \tag{8}$$

Table 1. An example of the calculation of the standard uncertainty $u(\sigma)$, using equation (14). Shown are individual uncertainty components contributing to the standard uncertainty of the total electron scattering cross section, σ, of Ne at $T = 100$ eV.

Variable w_υ	Value	$u(w_\upsilon)$	$\xi_\upsilon = \partial\sigma/\partial w_\upsilon$	$u_\upsilon \equiv \lvert\xi_\upsilon\rvert u(w_\upsilon)$
k_1	1	1.0×10^{-3}	3.05×10^{-16} cm^2	3.05×10^{-19} cm^2
k_2	1	0	3.05×10^{-16} cm^2	0
k_3	1	1.0×10^{-2}	3.05×10^{-16} cm^2	3.05×10^{-18} cm^2
m	3.051×10^{-16} cm^2	1.8×10^{-18} cm^2	1	1.8×10^{-18} cm^{-2}
T	100 eV	0.3 eV	1.0×10^{-19} cm^2 eV^{-1}	3.0×10^{-20} cm^{-2}
σ				3.6×10^{-18} cm^2

respectively, with

$$q_0 = (c_0 - c_{off})/I_0, \tag{9}$$

$$q = (c - c_{off})/I, \tag{10}$$

$$n_e L = \frac{p\chi_B}{k_B\Theta}\sqrt{\frac{\Theta}{\Theta_c}}L + \varepsilon_1 + \varepsilon_2 \equiv nL + \varepsilon_1 + \varepsilon_2. \tag{11}$$

In equation (7), the term a_i was added to account for a potential offset in a plot of $\ln(q/q_0)$ versus nL, which may arise for several reasons, for instance due to a shift of the zero point of the manometer reading or of the electron detection electronics. The quantity c_{off} is the background count rate of the channel electron multiplier, which was in the first order independent of the pressure p. I_0 and I are the electron beam current at the entrance aperture of the scattering cell when the cell is empty and filled with the gas of the number density n, respectively. The normalization of the net count rate $c - c_{off}$ to the electron beam current I was performed to correct for the change of the count rate due to an alteration of the primary electron beam current during the measurement.

In practice, the real number of gas atoms per area differs from nL, which was determined by means of the ideal gas law because of a few experimental effects. In order to take into account these effects, equation (11) was inserted, where the real number of gas atoms per area, denoted by n_eL, was calculated by adding up the main component, nL, and the two minor terms, ε_1 and ε_2. The quantity χ_B denotes the correction factor for the reading value of our capacitance manometer shown in figure 2. The correction factor was multiplied by $(\Theta/\Theta_c)^{1/2}$, to account for the shift of the manometer reading due to the fact that the gas temperature $\Theta_c = 23.7\,^\circ$C at the time of the comparison with the pressure standards was different from that during the present measurement.

The term ε_1 corrects for the inhomogeneity of the number density near the apertures of the scattering cell caused by atoms effusing through the apertures and is given by

$$\varepsilon_1 = \int_{-\infty}^{\infty} \tilde{n}(z)\,\mathrm{d}z - nL, \tag{12}$$

where $\tilde{n}(z)$ is the number density distribution of gas atoms along the z axis, which coincides with the beam axis. The value of the correction term ε_1 was estimated using the numerical data given in table 1 in the work of Mathur *et al* (1975). It amounts to $3.0 \times 10^{-3} \times nL$.

The term ε_2 accounts for the additional attenuation of electrons in the energy analyser and is given by

$$\varepsilon_2 = \frac{p_A\chi_i}{k_B\Theta} l \frac{\sigma_A}{\sigma}, \tag{13}$$

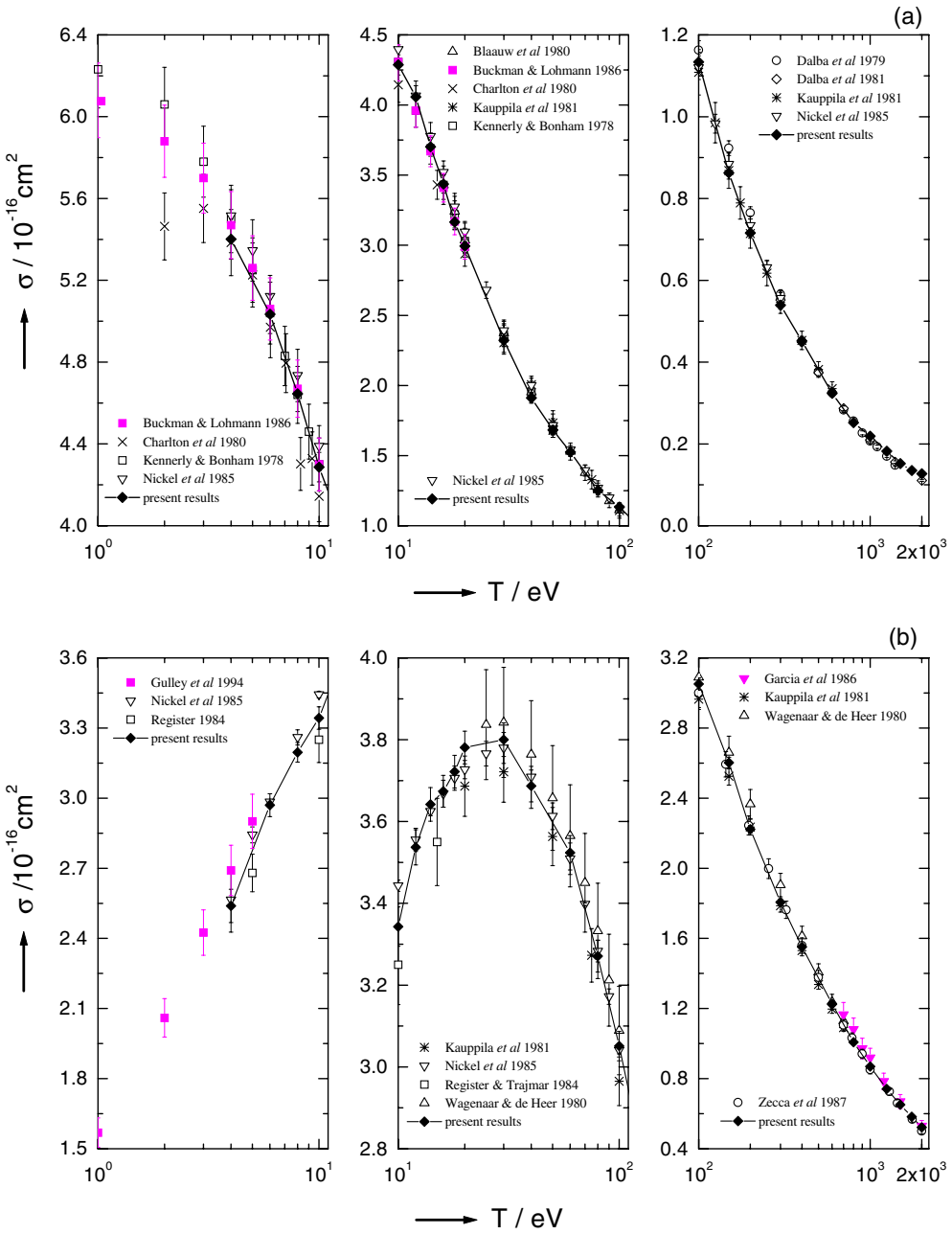

Figure 6. Total electron scattering cross sections σ of (a) He, (b) Ne and (c) Ar as a function of electron energy T. The results of the present experiment are shown in comparison with the data of other authors.

where p_A is the gas pressure in the analyser measured by an ionization vacuum gauge, χ_i the correction factor for the reading of this vacuum gauge, which depends on the gas type, l the length of the electron path in the analyser and σ_A the total electron scattering cross section of

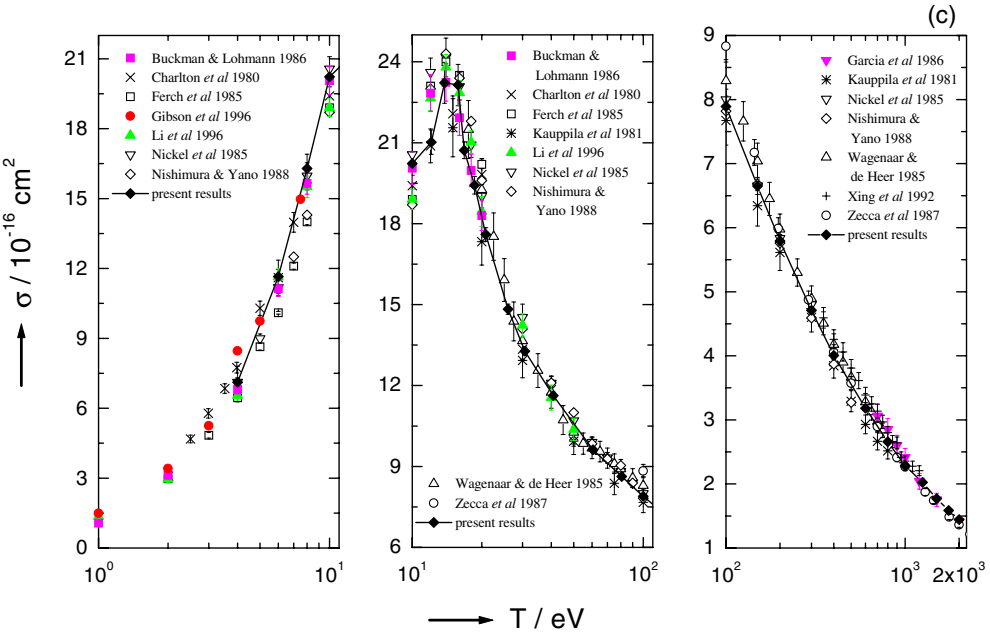

Figure 6. (Continued.)

the measuring gas at the pass energy of the analyser, which is usually chosen several times smaller than the primary electron energy, to obtain a higher energy resolution. The adjustment of the pass energy of the analyser was achieved by varying the retarding field applied to the entrance slit of the analyser.

Since X_i as well as Y_i are functions of quantities which are subject to experimental uncertainties, we are faced with a regression analysis involving uncertainties in both coordinates. Bruzzone and Moreno (1998) noted in their recent publication that a linear regression analysis using the standard version, i.e. considering only the uncertainties in the y coordinate and disregarding those in the x coordinate, may in some situations lead to a considerable distortion of fitting results. In view of this fact, the fitting parameters a_i and m_i were determined by means of a linear regression analysis taking into account the uncertainties in both coordinates. For this purpose, the algorithms of Reed (1992) were employed, which enable us to compute the values as well as the uncertainties of the parameters a_i and m_i using analytical expressions in terms of the values of the two variables and their uncertainties. A description of the formula used in the fitting procedure is given in the appendix.

The values and the uncertainties of m_i obtained by the linear regression analysis were inserted in equation (6) to compute the weighted average $m(T)$ and then the final result $\sigma(T)$, according to equations (3)–(5). The standard uncertainty, $u(\sigma)$, of $\sigma(T)$ was calculated from equation (3), using the law of propagation of uncertainty:

$$u^2(\sigma) = \left(\frac{\partial\sigma}{\partial k_1}\Delta k_1\right)^2 + \left(\frac{\partial\sigma}{\partial k_2}\Delta k_2\right)^2 + \left(\frac{\partial\sigma}{\partial k_3}\Delta k_3\right)^2 + \left(\frac{\partial\sigma}{\partial m}\Delta m\right)^2 + \left(\frac{\partial\sigma}{\partial T}\Delta T\right)^2, \tag{14}$$

where the uncertainty, Δm, of the weighted mean, $m(T)$, is given by

$$(\Delta m)^2 = 1\Big/\sum_i 1/u^2(m_i). \tag{15}$$

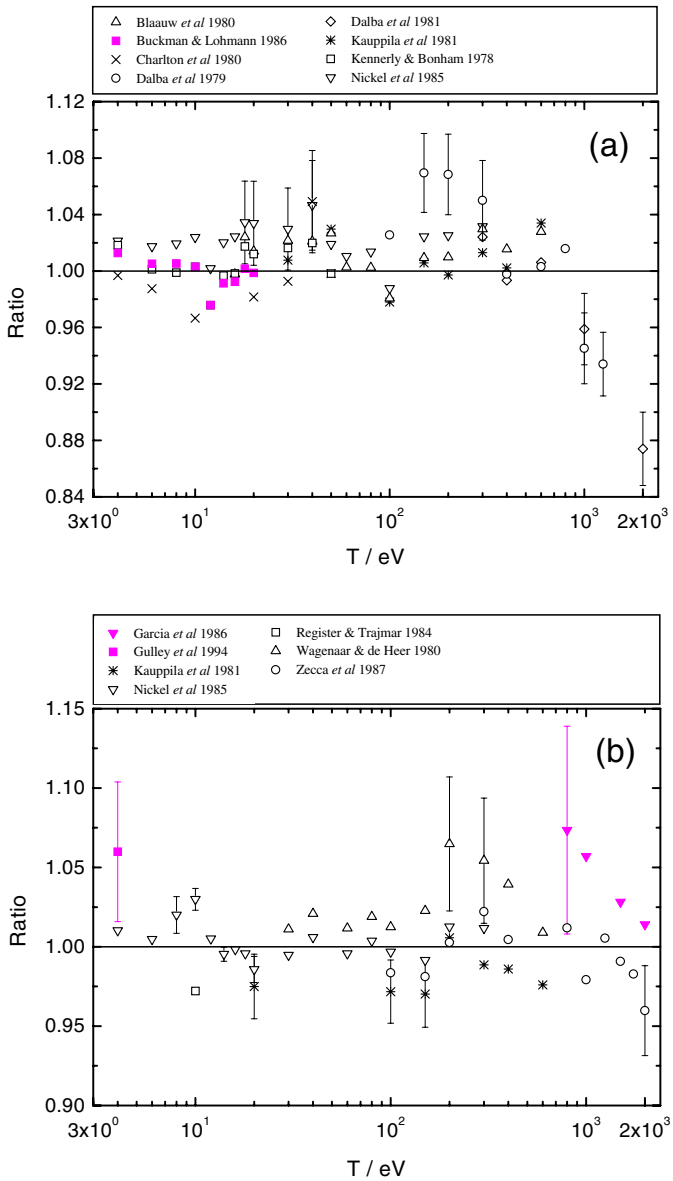

Figure 7. Ratios of the existing experimental data to the results of the present experiment for (a) He, (b) Ne and (c) Ar. The uncertainties of the ratios were obtained by the square root of the quadratic sum of the uncertainties of the present results and those of other authors. For the sake of clarity, the drawing of the error bars is omitted if the ratio deviates from unity by less than its uncertainty, in other words, if the present result agrees with the compared experimental data within the uncertainties. In the diagram for Ar, the uncertainties for the data of Nishimura and Yano (1988) are not plotted. They are in the order of 20%.

The last term on the right-hand side of equation (14) was added to account for the uncertainty ΔT in the electron beam energy. Instead of declaring the uncertainty in T, we converted it into the uncertainty of σ using its first derivative with respect to the beam energy. As an example, table 1 shows the summary of the uncertainty components of the total electron scattering cross section of Ne at $T = 100$ eV.

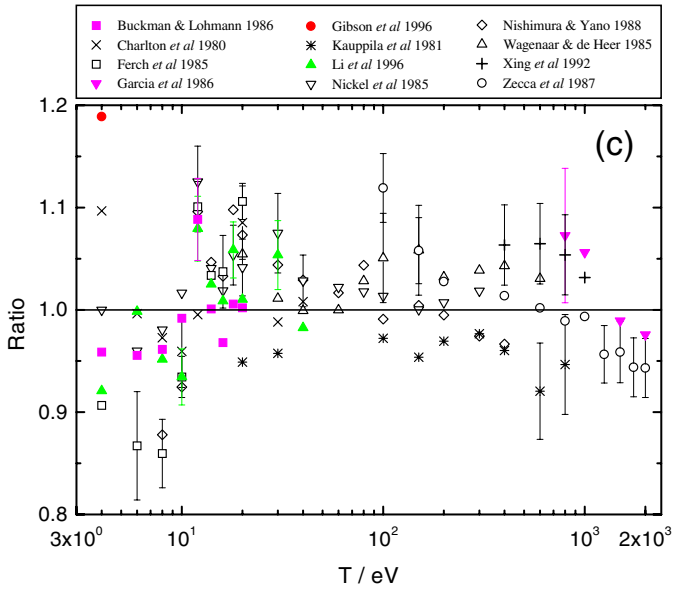

Figure 7. (Continued.)

5. Results and discussion

5.1. Comparison with other experimental data

The results of the present experiment are listed in table 2 and displayed in figures 6(a)–(c) in comparison with those of other authors. The relative deviations among the results of different authors can be seen in figures 7(a)–(c), where the ratios of the experimental data of other authors to our results are plotted as a function of energy. For the calculation of the ratios, interpolated values were employed when the energies of the original data were slightly different from those measured in the present work. It should be mentioned that the data of Gulley *et al* (1994), of Register and Trajmar (1984) for Ne and of Gibson *et al* (1996) for Ar are integral elastic scattering cross sections, which are equal to the total scattering cross sections if the energy is lower than the first excitation threshold in the respective atoms.

Figures 7(a)–(c) show that the results of the present work approximately represent the centre of the existing experimental data distribution throughout the energy range. Good agreement is found for the experimental results for He and Ne in the energy range below 600 eV. Here, the majority of the experimental data scatter around our results with relative deviations less than 4%, which is in the order of the uncertainties claimed by the authors. With the exception of the energy range below 10 eV, the experimental data of Ar also show satisfactory agreement, although the relative deviations here are somewhat larger than for He and Ne. However, the relative deviations in most cases do not exceed 7% and lie nearly within the range of the error bars. Much larger deviations are found in the energy region beneath the maximum of the total scattering cross section at 14 eV, where the total scattering cross section decreases by nearly two orders of magnitude from the maximum to the Ramsauer minimum at 0.345 eV. In this energy region, the relative deviations reach about 19%. The present results are in good agreement with the data of Nickel *et al* (1985), apart from the value at 12 eV. In the contrast to this, a serious disagreement was found between the results of the present work and those of Ferch *et al* (1985) at low energies. At 8 eV, for instance, our result is about

Table 2. Total electron scattering cross sections of He, Ne and Ar including the standard uncertainties determined using equation (14).

Helium		Neon		Argon	
T (eV)	σ (10^{-16} cm^2)	T (eV)	σ (10^{-16} cm^2)	T (eV)	σ (10^{-16} cm^2)
4	5.401 ± 0.098	4	2.539 ± 0.071	4	7.114 ± 0.685
6	5.034 ± 0.095	6	2.970 ± 0.049	6	11.648 ± 0.708
8	4.645 ± 0.087	8	3.196 ± 0.042	8	16.288 ± 0.617
10	4.287 ± 0.072	10	3.343 ± 0.048	10	20.227 ± 0.433
12	4.058 ± 0.080	12	3.537 ± 0.043	12.1	21.022 ± 0.451
14	3.702 ± 0.068	14	3.642 ± 0.041	13.8	23.219 ± 0.758
16	3.436 ± 0.065	16	3.674 ± 0.039	15.8	23.139 ± 0.767
18	3.165 ± 0.053	18	3.722 ± 0.040	16.8	20.720 ± 0.310
20	2.994 ± 0.048	20	3.781 ± 0.040	18.6	19.426 ± 0.326
30	2.322 ± 0.044	30	3.800 ± 0.041	20.8	17.601 ± 0.252
40	1.912 ± 0.033	40	3.687 ± 0.039	26.0	14.830 ± 0.186
50	1.683 ± 0.031	60	3.524 ± 0.042	30.7	13.276 ± 0.150
60	1.525 ± 0.032	80	3.271 ± 0.039	40.8	11.626 ± 0.131
80	1.252 ± 0.027	100	3.051 ± 0.036	60.6	9.619 ± 0.103
100	1.134 ± 0.024	150	2.602 ± 0.031	80.7	8.627 ± 0.091
150	0.863 ± 0.015	200	2.222 ± 0.023	100	7.891 ± 0.086
200	0.716 ± 0.013	300	1.806 ± 0.019	150	6.651 ± 0.072
300	0.539 ± 0.010	400	1.552 ± 0.016	200	5.790 ± 0.062
400	0.452 ± 0.011	600	1.227 ± 0.013	300	4.711 ± 0.052
600	0.324 ± 0.008	800	1.007 ± 0.011	400	4.004 ± 0.047
800	0.252 ± 0.005	1000	0.869 ± 0.010	600	3.183 ± 0.037
1000	0.219 ± 0.004	1250	0.741 ± 0.008	800	2.658 ± 0.033
1250	0.182 ± 0.003	1500	0.651 ± 0.007	1000	2.284 ± 0.027
1500	0.152 ± 0.004	1750	0.582 ± 0.007	1250	2.024 ± 0.024
1750	0.135 ± 0.003	2000	0.522 ± 0.007	1500	1.770 ± 0.021
2000	0.127 ± 0.003			1750	1.585 ± 0.019
				2000	1.444 ± 0.018

14% higher than that of Ferch *et al* (1985). The reason for these discrepancies is not clear. Furthermore, the data of Gibson *et al* (1996), who obtained the integral elastic scattering cross sections using phaseshift analysis (Allen 1986), are at 4 eV about 19% higher than the present result. As can be seen from figure 6(c), however, their value at 4 eV is questionable, because it is significantly higher than that to be expected from a smooth energy dependence of the total scattering cross section in the energy region.

A striking systematic deviation can be observed when comparing our results with the data of the Trento group, i.e. the data of Dalba *et al* (1979, 1981) and Zecca *et al* (1987). This can clearly be seen in the data for He. As figure 7(a) shows, the ratios of the results of the Trento group to those of the present work for He exhibit a monotonic decrease with increasing electron energy. Below 600 eV our values are smaller than those of the Trento group, whereas above 600 eV our results are significantly higher. The relative difference amounts to 4% at 1000 eV and increases to 13% at 2000 eV. As can be seen from figures 7(b) and (c), similar energy-dependent deviations can also be observed for the gases Ne and Ar, although the differences are smaller than for He.

When looking for the potential reasons for the large deviations found between the present results and the data of the Trento group, we first checked the purity of the measuring gas using a quadrupole mass filter, because a contamination by atmospheric gases can lead to a substantial

rise of the measured cross sections, especially for helium, whose total electron scattering cross sections are smaller than those of N_2 by about one order of magnitude. The analysis of the mass spectrum revealed that the concentration of atmospheric gases is lower than 0.1%, which is too small to explain the deviation in the order of 10%.

It is well known that an imperfect separation of electrons scattered in the forward direction is one of the major error sources in the measurement of total electron scattering cross sections at high electron energies. It causes a reduction of the measured value of total electron scattering cross section from the true value. The higher the electron energy, the larger the fraction of the forward-scattered electrons. Consequently, the reduction increases with increasing electron energy, as the data of the Trento group do in relation to the present results. We therefore suppose that the deviation between our results and the data of the Trento group is due to different levels of the separation of the forward-scattered electrons.

In the present experiment, the energy and the average angular resolution of the electron energy analyser were better than 1 eV and 0.7°, respectively. The energy resolution is much smaller than the lowest excitation energy in the three noble-gas atoms and, therefore, a reduction of the total scattering cross sections due to interference by electrons scattered inelastically can be ruled out. In comparison to inelastic scattering, the cross sections for elastic scattering change rather slowly with the scattering angle at high energies, so that the fraction of the electrons scattered into the range of our angular resolution, i.e. 0°–0.7°, is negligibly small. As described above, the reduction of our total scattering cross sections due to interference by electrons scattered elastically in the forward direction is smaller than 0.1%.

The determination of energy and angular resolution of a Ramsauer spectrometer, as used by the Trento group, is more complicated than in the present case, because of the presence of the bending magnetic field throughout the scattering and detection area. The Trento group stated 1% as the relative energy resolution of their apparatus, 0.7° as the angular resolution for the He measurement and 0.4° for the measurement of Ne and Ar, which were defined by three slits placed in the gap between scattering cell and detector. It appears, however, that in their estimate they did not consider the enhanced deflection of those electrons by the bending magnetic field, which lose part of their energy by inelastic scattering. A numerical simulation of the electron trajectories in the Ramsauer spectrometer revealed, for instance, that electrons with the primary energy of 1 keV could pass through the slit system used by the Trento group and reach the detector, if they were scattered into the angle of 1.2° with an energy loss of 50 eV, which are clearly outside the energy and angular resolution stated by the Trento group. This means that the real fraction of the scattered electrons reaching the detector should be much higher than that estimated by the Trento group and supports the assumption that the deviations between the present results and their data arise from the imperfect separation of the scattered electrons in the latter experiment.

The fact that the deviation in the case of He is greater than for the other two gases is also consistent with the spectral distribution of the optical oscillator strengths in the three atoms, which are related to the differential electron scattering cross sections with respect to the scattering angle and secondary electron energy within the framework of the Born approximation. In the energy loss spectra of He, a strong peak can be observed at the energy loss value of 21.22 eV, due to the excitation $1^1S \rightarrow 2^1P$. The contribution of this transition to the total electron scattering cross section of He is significantly greater than that of excitations into the discrete and continuum states in Ne and Ar in the excitation-energy range 10–30 eV. In other words, imperfect separation of electrons scattered inelastically with an energy loss of 10–30 eV would lead, in relative terms, to the measured total electron scattering cross sections of He being reduced more strongly than in the case of Ne and Ar, in accordance with the deviations between the results of the present work and those of the Trento group for the three

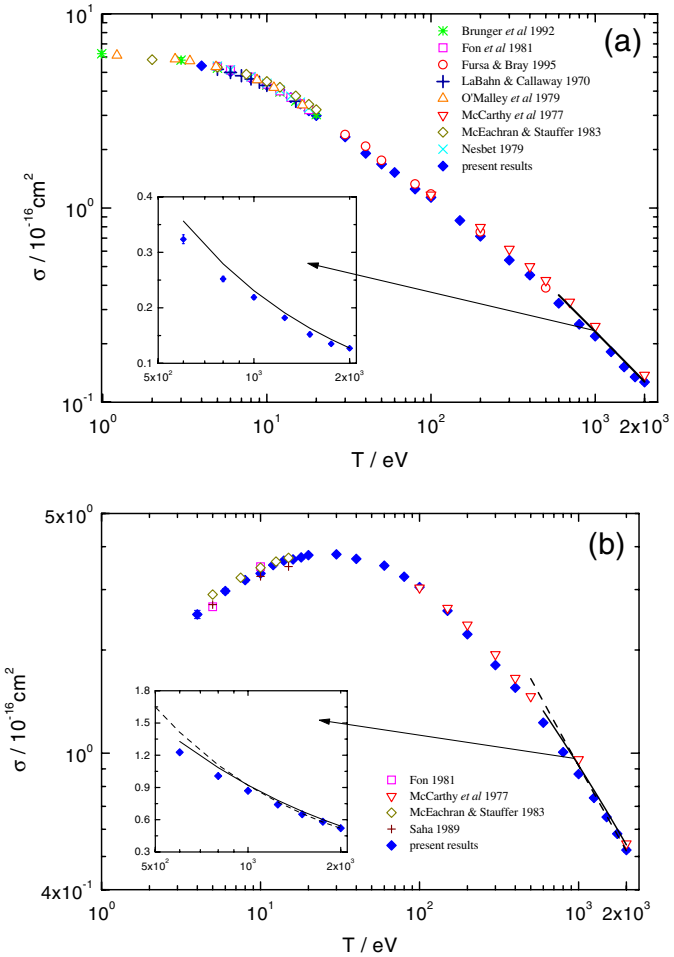

Figure 8. Comparison of the results of the present experiment with those of theoretical calculations for (a) He, (b) Ne and (c) Ar. The solid curve (——) represents the total scattering cross sections obtained by adding the integral elastic scattering cross sections of Mayol and Salvat (1997) and the integral inelastic scattering cross sections calculated using equation (16), where the values of the parameter M^2_{tot} amounted to 0.7525, 1.924 and 4.409 for He, Ne and Ar, respectively. The values of C_{tot} were 8.07 for He, 19.31 for Ne and 47.72 for Ar. The dashed curve (– – –) in (b) and (c) depicts the total scattering cross sections determined using the semi-empirical formula of Garcia *et al* (1999). The total scattering cross sections of Ar based on the semi-empirical integral inelastic scattering cross sections of de Heer *et al* (1979) are described by the dotted curve (· · · · · ·). The high-energy parts of the figures are drawn once again in the inserted boxes. The uncertainty of the data of Gibson *et al* (1996) for Ar is not known and therefore not drawn in (c).

gases. It should be noted that our results do not show a clear systematic deviation from the data of Garcia *et al* (1986). In their recent paper, Zecca *et al* (2000) recognized that part of the discrepancies between the results of the Trento group and those of Garcia *et al* (1986) can be explained by the poorer separation of electrons inelastically scattered by the Trento apparatus.

5.2. Comparison with theoretical calculations

In parallel to the experimental studies, a great deal of theoretical work has been carried out with regard to electron scattering by light noble-gas atoms, leading to significant progress in the

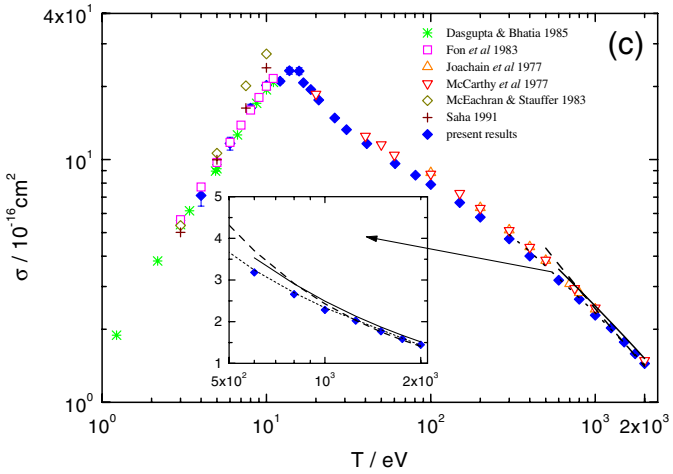

Figure 8. (Continued.)

development of theoretical approaches for the description of electron-scattering processes. In the case of elastic scattering, a number of the theoretical approaches were able to reproduce the experimental scattering cross sections within a few per cent. In the case of inelastic scattering, the situation is less satisfactory, as there are considerable discrepancies between theoretical and experimental results, with the exception of the high-energy region, where the scattering cross sections are generally well predicted by the Bethe–Born approximation. In comparing with the theoretical results, we therefore focus on the energy range below the first excitation threshold, where the total scattering cross section is equal to the integral elastic scattering cross section because of the absence of inelastic scattering processes, and on the high-energy region, where the Bethe–Born approximation is applicable.

The major problem in calculating the elastic scattering cross sections for low-energy electrons consists in the accurate description of the dynamical-polarization effect of the target atoms due to incident electrons. The various existing theoretical approaches differ mainly in how this effect is taken into account in the calculation. The customary approaches are the polarized-orbital approximation (Temkin 1957, 1959), the optical-potential method (McCarthy *et al* 1977), the *R*-matrix method (Berrington *et al* 1974) and the multiconfiguration Hartree–Fock method (Saha 1989).

For helium, the integral elastic scattering cross sections below the first excitation threshold were calculated by Fon *et al* (1981) using the *R*-matrix method, by McEachran and Stauffer (1983a) using the adiabatic-exchange approximation, by LaBahn and Callaway (1970) applying the polarized-orbital method, by Nesbet (1979) using the matrix variational method and recently by Brunger *et al* (1992) employing the coupled channel optical model. These approximations were also used for the calculation of the integral elastic scattering cross sections of Ne and Ar: the *R*-matrix method for Ne and Ar by Fon *et al* (1981, 1983), the adiabatic-exchange approximation for Ne and Ar by McEachran and Stauffer (1983b), the polarized-orbital method for Ar by Dasgupta and Bhatia (1985) and the multiconfiguration Hartree–Fock method for Ne and Ar by Saha (1989, 1991). It should be noted that most of the authors calculated differential elastic scattering cross sections, from which the integral cross sections were obtained by the integration over the scattering angle.

Unfortunately, the majority of the theoretical works on the inelastic scattering deals with the excitation into selected discrete states, whose cross sections makes up only a small part

of the integral inelastic scattering cross section. To our knowledge, there exist only a few theoretical works where the integral cross sections are reported: McCarthy *et al* (1977) also applied the optical-potential method for inelastic scattering and calculated differential inelastic scattering cross sections of the three gases at electron energies from 20 to 3000 eV. The same method was used by Joachain *et al* (1977) to compute the total scattering cross sections of Ar in the energy range from 100 to 1000 eV. Fursa and Bray (1995) calculated the total electron scattering cross sections of He for electron energies from 30 to 500 eV, using the so-called convergent close-coupling method (Bray and Stelbovics 1992), which produced reliable results in the case of electron scattering by hydrogenic atoms and ions (Bray and Stelbovics 1995).

Making use of the Bethe–Born approximation and the sum rule, Inokuti *et al* (1967) showed for He that the integral inelastic scattering cross sections, σ_{in}, for electron energies down to 300 eV can be described by

$$\sigma_{in} = \frac{8\pi a_0^2 z_e^2}{m_e v_e^2/R}\left\{M_{tot}^2\left[\ln\left(\frac{\beta^2}{1-\beta^2}\right)-\beta^2\right]+C_{tot}\right\}, \tag{16}$$

where a_0 is the Bohr radius, z_e the electron charge, v_e the velocity of the incident electron, R the Rydberg energy and β the ratio of v_e to the light velocity. Quantities M_{tot}^2 and C_{tot} are parameters reflecting the influence of the target-atom structure on the scattering process, where M_{tot}^2 is a constant expressing the departure of the energy dependence of σ_{in} from T^{-1}. In the following, the present results above 500 eV will be examined with respect to the conformity with the Bethe–Born approximation using the theoretical values of M_{tot}^2 and C_{tot}.

In figures 8(a)–(c), the results of the present experiment are compared with the theoretical values. As figure 8(a) shows, there is an excellent agreement between the present results and the theoretical integral elastic scattering cross sections of He below 20 eV. Here, the differences are smaller than the symbol size. At higher energies, theoretical total scattering cross sections were determined by adding the theoretical integral inelastic scattering cross sections to the integral elastic scattering cross sections which were taken from the work of Mayol and Salvat (1997). It can be seen from figure 8(a) that the total scattering cross sections based on the inelastic scattering cross sections of Fursa and Bray (1995) fit well to the present data, while those derived using the inelastic scattering cross sections of McCarthy *et al* (1977) are generally about 11% higher than the present results. However, the energy dependence of the latter agrees well with that of the present experiment. Figure 8(a) further shows that the present results are rather well reproduced if the integral inelastic scattering cross sections of He are calculated using the Bethe–Born approximation with $M_{tot}^2 = 0.7525$ and $C_{tot} = 8.07$ (Inokuti *et al* 1975). Here, the agreement is better for higher electron energy, in accordance with the fact that the accuracy of the Bethe–Born approximation increases with rising energy.

As figures 8(b) and (c) show, the present results for Ne and Ar below the first excitation threshold also agree well with the theoretical data, except with those of McEachran and Stauffer (1983b) for Ar, which are about 35% higher than the present result at 10 eV. Above the first excitation threshold, McCarthy *et al* (1977) and Joachain *et al* (1977) calculated the integral inelastic scattering cross sections of Ne and Ar. The theoretical total scattering cross sections based on their cross sections are up to about 11% higher than the results of the present work, which is, however, not serious if one considers the uncertainty of the present results of a few per cent and that of the integral elastic scattering cross sections of 5% (Mayol and Salvat 1997). In figures 8(b) and (c), the present results for Ne and Ar are further compared with the theoretical total scattering cross sections derived using the Bethe–Born approximation, where the parameter values M_{tot}^2 and C_{tot} required for the calculation of σ_{in} were again taken from literature: $M_{tot}^2 = 1.924$ and $C_{tot} = 19.31$ for Ne (Inokuti *et al* 1975), and $M_{tot}^2 = 4.409$ and $C_{tot} = 47.72$ for Ar (Eggarter 1975). As in the case of He, the present results accord rather

well with the theoretical total scattering cross sections based on the Bethe–Born approximation above 1 keV, whereas there are noticeable deviations between them at lower energies. The deviations increase with decreasing electron energy.

In their recent paper, Garcia *et al* (1999) gave a semi-empirical formula for the total electron scattering cross sections of Ne and Ar in the energy range 0.5–10 keV. They derived the semi-empirical formula from the experimental total scattering cross sections (Garcia *et al* 1986) and those calculated using the Bethe–Born approximation. Based on the finding that the difference between their experimental and theoretical total scattering cross sections decreases exponentially with the electron energy, they proposed a semi-empirical formula which complies with the Bethe–Born approximation at high energies. It can be seen from figures 8(b) and (c) that the energy dependence of the semi-empirical formula is different from that of the present results. The present results for Ne and Ar are in good agreement with the semi-empirical formula above 1 keV but noticeably smaller than those predicted by the semi-empirical formula below 1 keV. For the sake of completeness, the present results for Ar are also compared with the total scattering cross sections obtained using the semi-empirical integral inelastic scattering cross sections of de Heer *et al* (1979). It can be seen from figure 8(c) that the two cross sections also agree very well at energies below 1 keV.

6. Conclusions

Total electron scattering cross sections of He, Ne and Ar were measured for electron energies from 4 to 2000 eV with uncertainties which are generally smaller than 3%. For the electron energies below 600 eV, our results agree relatively well with the experimental data of other authors, with the exception of the argon data in the energy range 4–10 eV, where the data of Ferch *et al* (1985) and Charlton *et al* (1980) differ from the present results by up to about 13%, while those of Nickel *et al* (1985) agree well with the values obtained in this experiment. At energies above 600 eV, a systematic deviation between the results of the present work and those of the Trento group was observed. We attribute this deviation to insufficient separation of the scattered electrons in the experiment of the Trento group.

A good agreement was found between the theoretical integral elastic scattering cross sections and the results of the present work below the first excitation threshold for all three gases with only one exception. In the intermediate energy range, the theoretical total scattering cross sections based on the convergent close-coupling calculations of Fursa and Bray (1995) for He reproduce the present results surprisingly well, while those of He, Ne and Ar based on the calculations of McCarthy *et al* (1977) and Joachain *et al* (1977) show deviations of up to 11% from the present results, which are, however, tolerable when regarding the uncertainties of the experimental and the theoretical total scattering cross sections. A satisfactory agreement with the Bethe–Born approximation could be found for all three gases above 500 eV. Compared with the total scattering cross sections of Ne and Ar predicted by the semi-empirical formula of Garcia *et al* (1999), the present results tend to be smaller below 1 keV but agree well at higher energies.

Acknowledgments

The authors wish to thank the technical staff for their valuable technical assistance. This work was supported by the European Community within the Fourth Framework Programme of the Nuclear Fission Safety Research and Training Programme under contract no FI4P-CT96-0044 (radiation quality active monitoring based on nanometric measurements).

Table A.1. Contribution of the uncertainty, $u(w_\upsilon)$, of the variable w_υ to the uncertainty of x_j. The background count rate, c_{off}, amounts to 100 s^{-1}.

Variable w_υ	Source of uncertainty	Value of standard uncertainty $u(w_\upsilon)$	Sensitivity coefficient $\xi_{j\upsilon} = \partial x_j / \partial w_\upsilon$	Uncertainty component $u_{j\upsilon} \equiv \lvert\xi_{j\upsilon}\rvert u(w_\upsilon)$
χ_B	Calibration uncertainty	$5 \times 10^{-3} \times \chi_B$	$\frac{nL}{\chi_B}$	$5 \times 10^{-3} \times nL$
p	Reading uncertainty	$5 \times 10^{-3} \times p$	$\frac{nL}{p}$	$5 \times 10^{-3} \times nL$
Θ	Variation of room temperature	0.5 K	$-\frac{1}{2}\frac{nL}{\Theta}$	$\frac{1}{2}\frac{nL}{\Theta} \times 0.5$ K
L	Reading uncertainty	0.6 mm	n	$4.5 \times 10^{-3} \times nL$
ε_1	Uncertainty in the density distribution $\tilde{n}(z)$	$2 \times 10^{-3} \times nL$	1	$2 \times 10^{-3} \times nL$
ε_2	Reading uncertainty	$1 \times 10^{-3} \times nL$	1	$1 \times 10^{-3} \times nL$
x_j				$u_{x_j} = \sqrt{\sum_i u_{j\upsilon}^2}$

Appendix

Since the procedure for the linear regression analysis is the same for all measurement cycles, the index i denoting the measurement cycle in equation (7) is omitted in the following for the sake of simplicity. The aim of the linear regression analysis is to find the values of the parameters a and m that yield the best fit of the equation

$$Y = a - mX \tag{A.1}$$

to the experimental data. In the present work, we employ the York solution (York 1966), according to which the best fit is found by minimizing the sum, S, of the weighted squared residuals:

$$S = \sum_{j=1}^{N} [W(x_j)(x_j - X_j)^2 + W(y_j)(y_j - Y_j)^2], \tag{A.2}$$

where $W(x_j)$ and $W(y_j)$ are weighting factors for the data points x_j and y_j, respectively, and X_j and Y_j are the data values given by the best-fit equation. As usual, we use the inverses of the variances, $u_{x_j}^2$ and $u_{y_j}^2$, of x_j and y_j as the respective weighting factors, $W(x_j)$ and $W(y_j)$:

$$W(x_j) = 1/u_{x_j}^2 \qquad \text{and} \qquad W(y_j) = 1/u_{y_j}^2. \tag{A.3}$$

According to Reed (1992), the sum, S, is minimal when the slope, m, fulfils the following equation:

$$m^2\left(\sum \frac{W_j^2 U_j V_j}{W(x_j)}\right) - m\sum W_j^2\left(\frac{U_j^2}{W(y_j)} - \frac{V_j^2}{W(x_j)}\right) - \left(\sum \frac{W_j^2 U_j V_j}{W(y_j)}\right) = 0 \tag{A.4}$$

with

$$W_j = \frac{W(x_j)W(y_j)}{m^2 W(y_j) + W(x_j)}, \tag{A.5}$$

$$U_j = x_j - \sum W_j x_j \left(\sum W_j\right)^{-1}, \tag{A.6}$$

$$V_j = y_j - \sum W_j y_j \left(\sum W_j\right)^{-1}. \tag{A.7}$$

Table A.2. Contribution of the uncertainty, $u(w_\upsilon)$, of the variable w_υ to the uncertainty of y_j.

Variable w_υ	Source of uncertainty	Value of standard uncertainty $u(w_\upsilon)$	Sensitivity coefficient $\xi_{j\upsilon} = \partial y_j / \partial w_\upsilon$	Uncertainty component $u_{j\upsilon} \equiv \lvert\xi_{j\upsilon}\rvert u(w_\upsilon)$
c_0	Count-rate dependence of the detection efficiency	$10^{-2} \times c_0$	$-\dfrac{1}{c_0 - c_{off}}$	$\dfrac{10^{-2} c_0}{c_0 - c_{off}}$
c	Count-rate dependence of the detection efficiency	$10^{-2} \times c$	$\dfrac{1}{c - c_{off}}$	$\dfrac{10^{-2} c}{c - c_{off}}$
c_{off}	Random effects	$10\ \mathrm{s}^{-1}$	$\dfrac{1}{c_0 - c_{off}} - \dfrac{1}{c - c_{off}}$	$\dfrac{10\ \mathrm{s}^{-1}}{c_0 - c_{off}} - \dfrac{10\ \mathrm{s}^{-1}}{c - c_{off}}$
I_0	Temperature sensitivity of picoammeter	$7 \times 10^{-3} \times I_0$	$\dfrac{1}{I_0}$	7×10^{-3}
I	Temperature sensitivity of picoammeter	$7 \times 10^{-3} \times I$	$-\dfrac{1}{I}$	7×10^{-3}
y_j				$u_{y_j} = \sqrt{\sum_i u_{j\upsilon}^2}$

Table A.3. A numerical example of table A.1. The data for the example were taken from the experimental data for 100 eV electrons in Ne at pressure $p = 2.0 \times 10^{-3}$ mbar, which corresponds to the number density per area of 6.2×10^{14} cm^{-2}.

Variable w_υ	Value	$u(w_\upsilon)$	$\xi_{j\upsilon} = \partial x_j / \partial w_\upsilon$	$u_{j\upsilon} \equiv \lvert\xi_{j\upsilon}\rvert u(w_\upsilon)$
χ_B	0.974	4.9×10^{-3}	6.4×10^{14} cm^{-2}	3.1×10^{12} cm^{-2}
p	1.99×10^{-3} mbar	1.0×10^{-5} mbar	3.1×10^{17} mbar^{-1} cm^{-2}	3.1×10^{12} cm^{-2}
Θ	298.2 K	0.5 K	-1.0×10^{12} K^{-1} cm^{-2}	5.0×10^{11} cm^{-2}
L	132 mm	0.6 mm	4.7×10^{13} cm^{-3}	2.8×10^{12} cm^{-2}
ε_1	1.9×10^{12} cm^{-2}	1.2×10^{12} cm^{-2}	1	1.2×10^{12} cm^{-2}
ε_2	1.9×10^{12} cm^{-2}	6.2×10^{11} cm^{-2}	1	6.2×10^{11} cm^{-2}
x_j	6.26×10^{14} cm^{-2}			5.4×10^{12} cm^{-2}

The variance, $u^2(m)$, of the slope, m, was computed via

$$u^2(m) = \sum_j \left[\frac{1}{W(y_j)} \left(\frac{\partial m}{\partial y_j} \right)^2 + \frac{1}{W(x_j)} \left(\frac{\partial m}{\partial x_j} \right)^2 \right], \tag{A.8}$$

where $(\partial m / \partial y_i)$ and $(\partial m / \partial x_i)$ were calculated using equations (A.1)–(A.11) given in the appendix of the work of Reed (1992).

The uncertainties of x_i and y_i were determined from those of the input quantities c_0, c, c_{off}, I_0, I, p, χ_B, L and Θ, and those of ε_1 and ε_2 in equations (8)–(11), according to the law of propagation of uncertainty. The uncertainties of all quantities are of type B, with the exception of those for c_0, c and c_{off}. The latter were estimated according to the type A method; in other words, they were set equal to the experimental standard deviations of the means calculated from a number of observations. Since the values of the correction terms, ε_1 and ε_2, were small compared to the main term, nL, we neglected the potential covariances and the sensitivity coefficients of the two terms with respect to other quantities. Tables A.1 and A.2 show the individual uncertainty components and their sensitivity coefficients, used to calculate the variances, $u_{x_j}^2$ and $u_{y_j}^2$, of the values of x_j and y_j, respectively, which enter into equation (A.3) for the determination of the weighting factors.

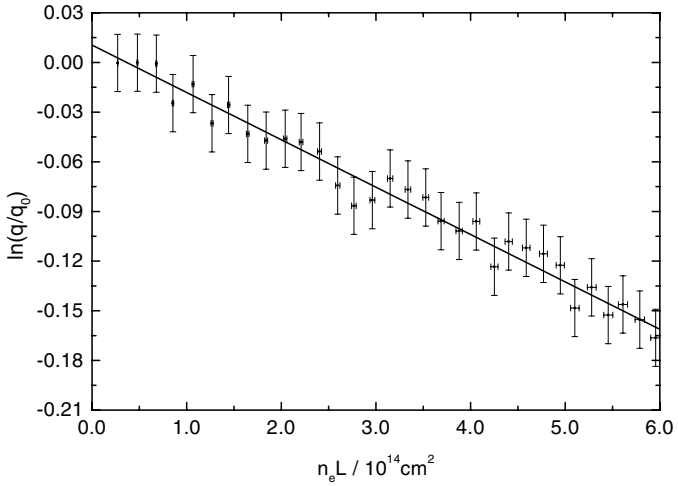

Figure A.1. An example of the linear regression analysis, taking into account uncertainties in both coordinates. The points with horizontal and vertical error bars are experimental data, representing the attenuation of 100 eV electrons in Ne. The result of the best fit is indicated by the unbroken line. For the sake of clarity, every second data point is not plotted.

Table A.4. A numerical example of table A.2. The example refers to the same experimental data as in table A.3.

Variable w_υ	Value	$u(w_\upsilon)$	$\xi_{j\upsilon} = \partial y_j / \partial w_\upsilon$	$u_{j\upsilon} \equiv \lvert\xi_{j\upsilon}\rvert u(w_\upsilon)$
c_0	32 266 s^{-1}	323 s^{-1}	3.1×10^{-5} s	1.0×10^{-2}
c	26 044 s^{-1}	260 s^{-1}	-3.9×10^{-5} s	1.0×10^{-2}
c_{off}	100 s^{-1}	10 s^{-1}	8.0×10^{-6} s	8.0×10^{-5}
I_0	0.291 pA	2×10^{-3} pA	-3.4 pA^{-1}	7.0×10^{-3}
I	0.285 pA	2×10^{-3} pA	3.5 pA^{-1}	7.0×10^{-3}
y_j	−0.1941			1.72×10^{-2}

Tables A.3 and A.4 show numerical examples of tables A.1 and A.2, where the data for the examples were taken from the experimental data for 100 eV electrons in Ne at the pressure $p = 2.0 \times 10^{-3}$ mbar, which corresponds to the number density per area of 6.2×10^{14} cm^{-2}. The weighting factors for other data points were calculated in a similar way and were then used to determine the best-fit values of the parameters a and m and their uncertainties, according to equations (A.3)–(A.8). A graphical example of the linear regression analysis is given in figure A.1, where a result of the best fit for 100 eV electrons in Ne is shown, together with the experimental data and their uncertainties.

References

Allen L J 1986 *Phys. Rev.* A **34** 2706–9

Berrington K A, Burke P G, Chang J J, Chivers A T, Robb W D and Taylor K T 1974 *Comput. Phys. Commun.* **8** 149–98

Blaauw H J, Wagenaar R W, Barends D H and de Heer F J 1980 *J. Phys. B: At. Mol. Phys.* **13** 359–76

Bransden B H and Joachain C J 1983 *Physics of Atoms and Molecules* (New York: Longman)

Bray I and Stelbovics A T 1992 *Phys. Rev. Lett.* **69** 53–6

Bray I and Stelbovics A T 1995 *Adv. At. Mol. Phys.* **35** 209–54

Brunger M J, Buckman S J, Allen L J, McCarthy I E and Ratnavelu K 1992 *J. Phys. B: At. Mol. Opt. Phys.* **25** 1823–38

Bruzzone H and Moreno C 1998 *Meas. Sci. Technol.* **9** 2007–11
Buckman S J and Lohmann B 1986 *J. Phys. B: At. Mol. Phys.* **19** 2547–64
Charlton M, Griffith T C, Heyland G R and Twomey T R 1980 *J. Phys. B: At. Mol. Phys.* **13** L239–44
Dalba G, Fornasini P, Lazzizzera I, Ranieri G and Zecca A 1979 *J. Phys. B: At. Mol. Phys.* **12** 3787–95
Dalba G, Fornasini P, Grisenti R, Lazzizzera I, Ranieri G and Zecca A 1981 *Rev. Sci. Instrum.* **52** 979–83
Dasgupta A and Bhatia A K 1985 *Phys. Rev.* A **32** 3335–43
de Heer F J, Jansen R H J and van der Kaay W 1979 *J. Phys. B: At. Mol. Phys.* **12** 979–1002
Edmonds T and Hobson J P 1965 *J. Vac. Sci. Technol.* **2** 182–97
Eggarter E 1975 *J. Chem. Phys.* **62** 833–47
Ferch J, Granitza B, Masche C and Raith W 1985 *J. Phys. B: At. Mol. Phys.* **18** 967–83
Fon W C and Berrington K A 1981 *J. Phys. B: At. Mol. Phys.* **14** 323–34
Fon W C, Berrington K A and Hibbert A 1981 *J. Phys. B: At. Mol. Phys.* **14** 307–21
Fon W C, Berrington K A, Burke P G and Hibbert A 1983 *J. Phys. B: At. Mol. Phys.* **16** 307–21
Fox R E, Hickam W M, Kieldaas T Jr and Grove D J 1951 *Phys. Rev.* **84** 859–60
Fursa D V and Bray I 1995 *Phys. Rev.* A **52** 1279–97
Garcia G, Arqueros F and Campos J 1986 *J. Phys. B: At. Mol. Phys.* **19** 3777–85
Garcia G, Roteta M, Manero F, Blanco F and Williart A 1999 *J. Phys. B: At. Mol. Opt. Phys.* **32** 1783–94
Gibson J C, Gulley R J, Sullivan J P, Buckman S J, Chan V and Burrows P D 1996 *J. Phys. B: At. Mol. Opt. Phys.* **29** 3177–95
Gulley R J, Alle D T, Brennan M J, Brunger M J and Buckman S J 1994 *J. Phys. B: At. Mol. Opt. Phys.* **27** 2593–611
International Organization for Standardization (ISO) 1993 *Guide to the Expression of Uncertainty in Measurement* (Geneva: ISO)
Inokuti M, Kim Y-K and Platzman R L 1967 *Phys. Rev.* **164** 55–61
Inokuti M, Saxon R P and Dehmer J L 1975 *Int. J. Radiat. Phys. Chem.* **7** 109–20
Joachain C J, Vanderpoorten R, Winters K H and Byron F W Jr 1977 *J. Phys. B: At. Mol. Phys.* **10** 227–38
Kauppila W E, Stein T S, Smart J H, Dababneh M S, Ho Y K, Downing J P and Pol V 1981 *Phys. Rev.* A **24** 725–42
Kennerly R E 1980 *Phys. Rev.* A **21** 1876–83
Kennerly R E and Bonham R A 1978 *Phys. Rev.* A **17** 1844–54
LaBahn R W and Callaway J 1970 *Phys. Rev.* A **2** 366–9
Li T, Fen A and Yang Y 1996 *Radiat. Phys. Chem.* **48** 711–14
Mathur B P, Field J E and Colgate S O 1975 *Phys. Rev.* A **11** 830–3
Mayol R and Salvat F 1997 *At. Data Nucl. Data Tables* **65** 55–154
McCarthy I E, Noble C J, Phillips B A and Turnbull A D 1977 *Phys. Rev.* A **15** 2173–85
McEachran R P and Stauffer A D 1983a *J. Phys. B: At. Mol. Phys.* **16** 255–74
McEachran R P and Stauffer A D 1983b *J. Phys. B: At. Mol. Phys.* **16** 4023–38
Nesbet R K 1979 *Phys. Rev.* A **20** 58–70
Nickel J C, Imre K, Register D F and Trajmar S 1985 *J. Phys. B: At. Mol. Phys.* **18** 125–33
Nishimura H and Yano K 1988 *J. Phys. Soc. Japan* **57** 1951–6
O'Malley T F O, Burke P G and Berrington K A 1979 *J. Phys. B: At. Mol. Phys.* **12** 953–65
Reed C B 1992 *Am. J. Phys.* **60** 59–62
Register D F and Trajmar S 1984 *Phys. Rev.* A **29** 1785–92
Saha H P 1989 *Phys. Rev.* A **39** 5048–61
Saha H P 1991 *Phys. Rev.* A **43** 4712–22
Temkin A 1957 *Phys. Rev.* **107** 1004–12
Temkin A 1959 *Phys. Rev.* **116** 358–63
Trajmar S and McConkey J W 1994 *Adv. At. Mol. Phys.* **33** 63–96
Wagenaar R W and de Heer F J 1980 *J. Phys. B: At. Mol. Phys.* **13** 3855–66
Wagenaar R W and de Heer F J 1985 *J. Phys. B: At. Mol. Phys.* **18** 2021–36
Xing S-L, Xu K-Z, Yang B-X, Chen X-J, Fan X-W, Wang Y-G and Zhang F 1992 *Chin. Sci. Bull.* **37** 1778–81
York D 1966 *Can. J. Phys.* **44** 1079–86
Zecca A, Karwasz G P and Brusa R S 1996 *Riv. Nuovo Cimento* **18** 1–146
Zecca A, Karwasz G P and Brusa R S 2000 *J. Phys. B: At. Mol. Opt. Phys.* **33** 843–5
Zecca A, Oss S, Karwasz G P, Grisenti R and Brusa R S 1987 *J. Phys. B: At. Mol. Phys.* **20** 5157–64